Chapter 4 Global climate change projections

4.1 Scenarios of greenhouse gas emissions, concentrations and radiative forcing

4.1.1 Emissions

The greenhouse gas emissions discussed here are those due to human activities, such as energy generation, transport, agriculture, land-clearing, industrial processes and waste. To provide a basis for estimating future climate change, the Intergovernmental Panel on Climate Change (IPCC 2000) prepared 40 greenhouse gas and sulfate aerosol emission scenarios for the 21st century that combine a variety of assumptions about demographic, economic and technological factors likely to influence future emissions. Each scenario represents a variation within one of four 'storylines': A1, A2, B1 and B2 (see Box 4.1). Projected carbon dioxide, methane, nitrous oxide and sulfate aerosol emissions based on these scenarios are shown in Figure 4.1.

Box 4.1 The IPCC Special Report on Emissions Scenarios (SRES) (IPCC 2000)

A1. The A1 storyline describes a future world of very rapid economic growth, a global population that peaks in mid-century and declines thereafter, and the rapid introduction of new and more efficient technologies. Major underlying themes are convergence among regions, capacity building and increased cultural and social interactions, with a substantial reduction in regional differences in per capita income. The A1 storyline develops into three scenario groups that describe alternative directions of technological change in the energy system. They are distinguished by their technological emphasis: fossil intensive (A1FI), non-fossil energy sources and technologies (A1T), or a balance across all sources (A1B) (where balanced is defined as not relying too heavily on one particular energy source, on the assumption that similar improvement rates apply to all energy supply and end use technologies).

A2. The A2 storyline describes a very heterogeneous world. The underlying theme is self reliance and preservation of local identities. Fertility patterns across regions converge very slowly, which results in continuously increasing population. Economic development is primarily regionally oriented and per capita economic growth and technological change more fragmented and slower than other storylines.

B1. The B1 storyline describes a convergent world with the same global population as in the A1 storyline (one that peaks in mid-century and declines thereafter) but with rapid change in economic structures toward a service and information economy, with reductions in material intensity and the introduction of clean and resource efficient technologies. The emphasis is on global solutions to economic, social and environmental sustainability, including improved equity, but without additional climate initiatives.

B2. The B2 storyline describes a world in which the emphasis is on local solutions to economic, social and environmental sustainability. It is a world with continuously increasing global population, at a rate lower than A2, intermediate levels of economic development, and less rapid and more diverse technological change than in the B1 and A1 storylines. While the scenario is also oriented towards environmental protection and social equity, it focuses on local and regional levels.

An illustrative scenario was chosen for each of the six scenario groups – A1B, A1FI, A1T, A2, B1 and B2. All were considered equally sound by the IPCC.

The SRES scenarios do not include additional climate initiatives, which means that no scenarios are included that explicitly assume implementation of the United Nations Framework Convention on Climate Change or the emissions targets of the Kyoto Protocol.

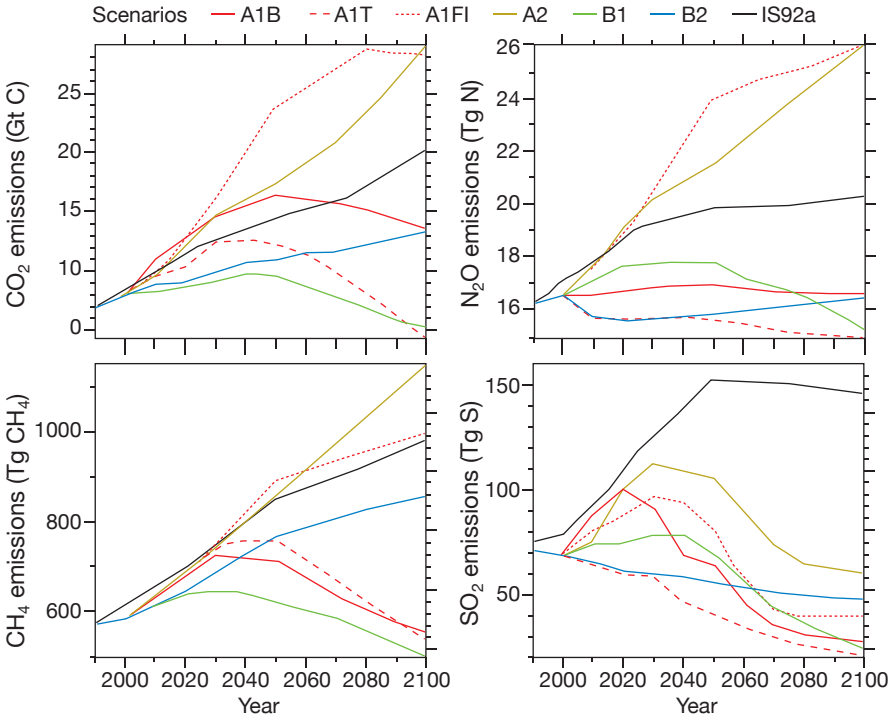

Figure 4.1: Anthropogenic emissions of carbon dioxide (CO_2), methane (CH_4), nitrous oxide (N_2O) and sulfur dioxide (SO_2) for six SRES scenarios (see Box 4.1) and the IS92a scenario from the IPCC Second Assessment Report in 1996 (IPCC 2001).

4.1.2 Concentrations

Carbon cycle models are used to convert emissions into atmospheric concentrations, allowing for uptake of emissions by the land and ocean, land and ocean climate feedbacks, and transport and chemical reactions in the atmosphere. The carbon dioxide (CO_2) lifetime in the atmosphere is difficult to quantify because it is continuously cycled between the atmosphere, ocean and biosphere, which involves a range of processes with different timescales. Around half the CO_2 emitted is removed on a time-scale of 30 years, a further 30% is removed within a few centuries, and the remaining 20% may stay in the atmosphere for thousands of years (Denman *et al*. 2007). Methane's atmospheric lifetime is about 8.4 years, nitrous oxide is around 114 years, 45 to 100 years for chlorofluorocarbons, 1 to 18 years for hydrochlorofluorocarbons and 1 to 270 years for hydrofluorocarbons (Denman *et al*. 2007).

Carbon cycle models give estimates of atmospheric CO_2 concentrations for the year 2100 ranging from 500 to 1200 ppm, compared to the 1990 concentration of 352 ppm (Meehl *et al*. 2007). Methane concentrations are projected to change from 1700 ppb in 1990 to 1400 to 3500 ppb by 2100, and nitrous oxide concentrations are projected to increase from 308 ppb in 1990 to 360 to 460 ppb by 2100 (Meehl *et al*. 2007). Concentrations of tropospheric ozone, hydrofluorocarbons and perfluorocarbons are also projected to increase.

Carbon cycle models project a reduction in the ability of the land and ocean to absorb anthropogenic CO_2, causing an increasingly large fraction of anthropogenic CO_2 to stay airborne. For example, for the A2 emission scenario, this positive feedback leads to additional atmospheric CO_2 concentration of 20 and 220 ppm by 2100 (Meehl *et al*. 2007).

This report does not explicitly address possible mitigation responses or pathways to greenhouse gas stabilisation as, by construction, none of the SRES factor in these issues (Box 4.1). However the lowest CO_2 emission scenario considered here, B1, peaks in mid-century, and declines thereafter to sufficient levels to come close to stabilisation of CO_2 concentrations (at around 550ppm) by century end. Methane and nitrous oxide concentrations also decrease and stabilise respectively over this period (refer to IPCC 2001 Technical Summary, p 65). To a first approximation, therefore, B1 may be considered representative of a stabilisation scenario to 550 ppm CO_2 by 2100. An important caveat on this is that carbon cycle feedbacks, which are currently very uncertain, must not be significantly larger than those considered in the original generation of this scenario (IPCC 2000). Details on mitigation pathways required for greenhouse gas stabilisation at a range of levels are given in the Working Group III contribution to the IPCC Fourth Assessment Report (IPCC 2007c).

4.1.3 Radiative forcing

Increasing concentrations of greenhouse gases affects the radiative balance of the Earth. The balance between incoming solar radiation and outgoing heat radiation defines the Earth's radiation budget (Bryant 1997). This balance determines the Earth's average temperature. Radiative forcing is the term given to an externally imposed change in the radiation balance, such as changes in atmospheric concentrations of greenhouse gases.

The greenhouse gas concentrations projected using the SRES are converted to a radiative forcing of the climate system using radiation codes (usually located within climate models themselves). Positive forcing warms the Earth, while negative forcing cools the Earth. CO_2 dominates the radiative forcing and has a warming effect. By the year 2100, the radiative forcing is about 4 Wm^{-2} for B1, 5 Wm^{-2} for A1T, 6 Wm^{-2} for B2, 7 Wm^{-2} for A1B, 8 Wm^{-2} for A2 and 9 Wm^{-2} for A1FI, compared to about 2 Wm^{-2} in 1990 (Fig 10.26 in Meehl *et al*. 2007).

Water vapour is another particularly important greenhouse gas. However direct human emissions of water vapour are negligible. Rather it is the *response* of water vapour to atmospheric warming which dictates its importance for climate change. A warmer atmosphere holds more water vapour, thereby increasing greenhouse trapping and resulting in further warming. This *positive feedback* therefore acts to amplify the warming initiated by increases in anthropogenic greenhouse gases such as carbon dioxide and methane.

4.2 Using global climate models to estimate future climate change

4.2.1 Global climate models

The complexity of processes in the climate system means we cannot simply extrapolate past trends to forecast future conditions. Climate models are the best tools we have for forecasting weather and climate. Perhaps the most familiar application is in daily weather forecasting. Models are also used for three-month climate forecasts for regions like Australia, which can assist agribusiness and other industries to plan for the months ahead. Another application is projecting the effect of human activities on climate over the coming decades, and explaining the causes of climate change over past decades. This includes increasing greenhouse gases and aerosols and stratospheric ozone depletion, e.g. the SRES (IPCC 2000) scenarios.

A climate model is a mathematical representation of the Earth's climate system. The mathematical equations are based on well-established laws of physics, such as conservation of mass, energy and momentum. They include the fact that the infrared radiation absorption bands are partially saturated, leading to a non-linear response to increasing greenhouse gas concentrations. The realism of climate models has been tested against a wealth of observational data from the natural world (for example, representation of spatial and temporal distribution of temperature, humidity, rainfall, pressure and winds). This provides a major source of confidence in the use of models for climate projection (see section 4.2.3). The ability of a model to simulate interactions in the climate system depends on the level of understanding of the geophysical and biochemical processes that govern the climate system. Our understanding of these processes has steadily improved, along with our ability to represent them in climate models. The increase in available computing power has allowed these processes to be represented in models with greater complexity and detail. Continued growth in computer power is essential for model improvement.

4.2.2 CMIP3 database of climate simulations

A new set of experiments from 23 models from research groups around the world is now available, representing a major advance for the evaluation of models and the generation of climate projections.

The availability of a new set of systematic model experiments from the Coupled Model Intercomparison Project 3 (CMIP3) database represents a major advance both for the evaluation of models and the generation of climate projections. The database includes more models (23) and more simulations of emission scenarios using each model. The model output is freely available to the research community, which has resulted in unprecedented levels of evaluation and analysis. The models in the CMIP3 database represent the current state-of-the-art in climate modelling, with generally more sophisticated representations of physical and dynamical processes, and finer spatial resolution.

The CMIP3 database provides monthly temperature and precipitation data for all 23 models. However, monthly data for other climate variables are available for *fewer* than 23 models, e.g. solar radiation for 20 models, wind speed for 17 models and relative humidity for 14 models (see Table 5.1 in Chapter 5). Some models have single simulations for the 20th and 21st centuries, while others have multiple simulations (ensembles). For models with multiple simulations, ensemble-mean changes in climate have been computed. The simulations of 20th century climate were driven by observed changes in greenhouse gases and aerosols. Some simulations included direct and indirect effects of anthropogenic aerosols, some included ozone depletion, and some included volcanic aerosols and solar forcing. Radiative forcing is not a directly observed quantity and is particularly uncertain for aerosols. Table 4.1 gives information about the various forcings used in each simulation and the spatial resolution of each model. The 21st century simulations were driven by the SRES A2 and A1B emission scenarios (IPCC 2000).

Table 4.1: The 23 global climate models used for simulations of 20th and 21st century climate, available from the CMIP3 database managed by the Program for Climate Model Diagnosis and Intercomparison (PCMDI) available at http://www-pcmdi.llnl.gov/ipcc/info_for_analysts.php. The reference numbers in column 1 are used in Table 5.1 in Chapter 5. The forcing factors are: G – Well-mixed greenhouse gases, O – Ozone, SD – Sulfate direct, SI – Sulfate indirect, BC – Black carbon, OC – Organic carbon, MD – Mineral dust, SS – Sea salt, LU – Land use, SO – Solar irradiance and V – Volcanic aerosol. Also given are global mean warming over the 21st century for the A1B emission scenario (see section 4.2.5; not available for BCCR model), and a skill score for Australia (see section 4.2.3).

No	Originating Group(s), Country	Model	Horizontal grid spacing (km)	Forcings used in model simulations	Warming (°C)	M Skill Score
1	Bjerknes Centre for Climate Research, Norway	BCCR	~175	G, SD	N.A.	0.590
2	Canadian Climate Centre, Canada	CCCMA T47	~250	G, SD	2.47	0.518
3	Canadian Climate Centre, Canada	CCCMA T63	~175	NOT AVAILABLE	3.03	0.478
4	Meteo-France, France	CNRM	~175	G, O, SD, BC	2.81	0.542
5	CSIRO, Australia	CSIRO-MK3.0	~175	G, O, SD	2.11	0.601
6	CSIRO, Australia	CSIRO-MK3.5	~175	G, O, SD	3.17	0.607
7	Geophysical Fluid Dynamics Lab, USA	GFDL 2.0	~200	G, O, SD, BC, OC, LU, SO, V	2.98	0.671
8	Geophysical Fluid Dynamics Lab, USA	GFDL 2.1	~200	G, O, SD, BC, OC, LU, SO, V	2.53	0.672
9	NASA/Goddard Institute for Space Studies, USA	GISS-AOM	~300	G, SD, SS	2.02	0.564
10	NASA/Goddard Institute for Space Studies, USA	GISS-E-H	~400	G, O, SD, SI, BC, OC, MD, SS, LU, SO, V	2.08	0.304
11	NASA/Goddard Institute for Space Studies, USA	GISS-E-R	~400	G, O, SD, SI, BC, OC, MD, SS, LU, SO, V	2.12	0.515
12	LASG/Institute of Atmospheric Physics, China	IAP	~300	G, SD	2.77	0.639
13	Institute of Numerical Mathematics, Russia	INMCM	~400	G, SD, SO	2.40	0.627
14	Institut Pierre Simon Laplace, France	IPSL	~275	G, SD, SI	3.19	0.505
15	Centre for Climate Research, Japan	MIROC-H	~100	G, O, SD, BC, OC, MD, SS, LU, SO, V	4.31	0.608
16	Centre for Climate Research, Japan	MIROC-M	~250	G, O, SD, BC, OC, MD, SS, LU, SO, V	3.35	0.608
17	Meteorological Institute of the University of Bonn, Meteorological Research Institute of KMA, Germany/Korea	MIUB	~400	G, SD, SI	2.97	0.632
18	Max Planck Institute for meteorology DKRZ, Germany	MPI-ECHAM5	~175	G, O, SD, SI	3.69	0.700
19	Meteorological Research Institute, Japan	MRI	~250	G, SD ,SO	2.52	0.601
20	National Center for Atmospheric Research, USA	NCAR-CCSM	~125	G, O, SD, BC, OC, SO, U	2.47	0.677
21	National Center for Atmospheric Research, USA	NCAR-PCM1	~250	G, O, SD, SO, V	1.96	0.506
22	Hadley Centre, UK	HADCM3	~275	G, O, SD, SI	3.12	0.608
23	Hadley Centre, UK	HADGEM1	~125	G, O, SD, SI, BC, OC, LU, SO, V	3.47	0.674

4.2.3 Reliability of climate models

Global climate models continue to improve in their ability to represent current global and regional patterns of temperature, precipitation and other variables. Simulation of major patterns of climatic variability particularly relevant to Australia (El Niño – Southern Oscillation, the Southern Annular Mode and the Madden-Julian Oscillation) have improved as well.

An important source of confidence in models comes from their ability to represent features of the current climate. Particularly important for Australia is how well climate models represent large-scale patterns of temperature, pressure and precipitation, as well as modes of variability such as the El Niño – Southern Oscillation (ENSO), the Southern Annular Mode and the Madden-Julian Oscillation, all of which affect regional climate.

Confidence in model projections varies with spatial and temporal scale. Highest confidence is attached to results analysed at the coarsest spatial and temporal scales, such as global or hemispheric annual means, and decreases with finer scales, such as sub-continental or regional daily variability. This is partly because the magnitude of natural variability increases as scales decrease, so that regional climate change signals are more easily masked by climate variability. Furthermore, local influences on climate (such as regional topography or processes) become more important at finer spatial scales.

Important physical processes that occur at scales too small to be explicitly resolved by the models are represented in approximate form as they interact with resolved scales (referred to as model 'parameterisations'). Examples include the interaction of radiation with atmospheric molecules and aerosols, convection within the atmosphere and ocean, small scale mixing by eddies and processes associated with the formation and dissipation of clouds. Our ability to parameterise such small-scale processes is imperfect, and different representations of those processes amongst models affect the magnitude and patterns of climate change projections. The response of clouds to climate change, in particular, is an important source of uncertainty in model projections (Soden and Held 2005). Nevertheless, this does not mean that models have no reliability at finer scales. Models can skillfully represent, for example, some types of temperature extreme – features intrinsically of small spatial and temporal scales (Tebaldi *et al*. 2007). Model resolution and parameterisations continue to improve, and several 'downscaling' techniques have been developed specifically to address regional and local climate change issues (see Chapter 5).

Mean global temperature errors from IPCC models are generally less than 3ºC outside polar regions (Figure 4.2). Greatest errors occur over land at high latitudes, likely due in part to elevation errors over ice sheets. Over the oceans, greatest relative errors occur over eastern ocean basins consistent with insufficient cloud in stratocumulus decks over cold water being simulated. Despite the errors, the typical pattern correlation coefficients between individual models and the observations are very high (0.98), indicating extremely good model representations of temperature distributions. This represents considerable improvement since the IPCC Third Assessment Report (IPCC 2001). The annual cycle in temperature is also well simulated, with mean errors in most regions less than 1ºC. Even over the Northern Hemisphere land mass, where annual temperature variations are very high, typical model errors are less than 2ºC (Randall *et al*. 2007). Although confidence is greatest for variables at the global and continental scale, some models can adequately represent the magnitude of temperature variability down to sub-continental scales (Karoly and Wu 2005).

Surface temperature patterns are driven largely by direct radiative forcing and land-sea temperature gradients. Mean precipitation patterns, on the other hand, more strongly reflect the general atmospheric circulation. Figure 4.3 shows that models represent overall features well, including the inter-tropical convergence zone, subtropical dry zones and general position of mid-latitude storm tracks. The details of those patterns, however, show a number of systematic errors that are potentially important to Australian projections. Many models show an unrealistic double inter-tropical convergence zone over the tropical Pacific, and the equatorial Pacific 'cold tongue' extends too far westward (Cai *et al*. 2003b,c; Dai 2006). Such errors in temperature and precipitation patterns also negatively affect the representation of the seasonal cycle and ENSO. Models generally also show too much light rain (1-10 mm per day) compared to observations, and underestimate the contribution and frequency for heavy rain (>20 mm per day; Watterson and Dix 2003; Dai 2006), likely to adversely affect projections of features such as heavy rain events. Recent increases in spatial resolution have, however,

improved the simulation of mid-latitude cyclones, and hence mid-latitude storm tracks (Bengtsson *et al*. 2006).

Significantly for simulation of variability in the Australian region, in recent years there has been an improvement in the ability of models to represent the spatial pattern and frequency of ENSO. For example, models are better able to reproduce the characteristic two-to-seven year frequency of ENSO. Problems remain, however, in simulating the asymmetry between El Niño and La Niña episodes, and the tendency for ENSO events to commence around March-May and persist through to December-February (Randall *et al*. 2007).

The importance of the Madden-Julian Oscillation for Australian regional climate includes its impact on tropical rainfall variability, onset and break events in the Australian monsoon, and possibly for its role in triggering ENSO events. Although models represent some gross features of Madden-Julian Oscillation variability, its magnitude is generally underestimated in the IPCC models (Lin *et al*. 2006), and errors persist in its structure and propagation (Hendon 2005). The Southern Annular Mode is a leading mode of extratropical variability in the southern hemisphere, and has important signatures on Australian rainfall. Models generally represent the spatial structure of Southern Annular Mode well (Cai *et al*. 2003a), although they differ in their ability to represent its amplitude and temporal and zonal structures (Raphael and Holland 2006). The IPCC Fourth Assessment Report concluded that

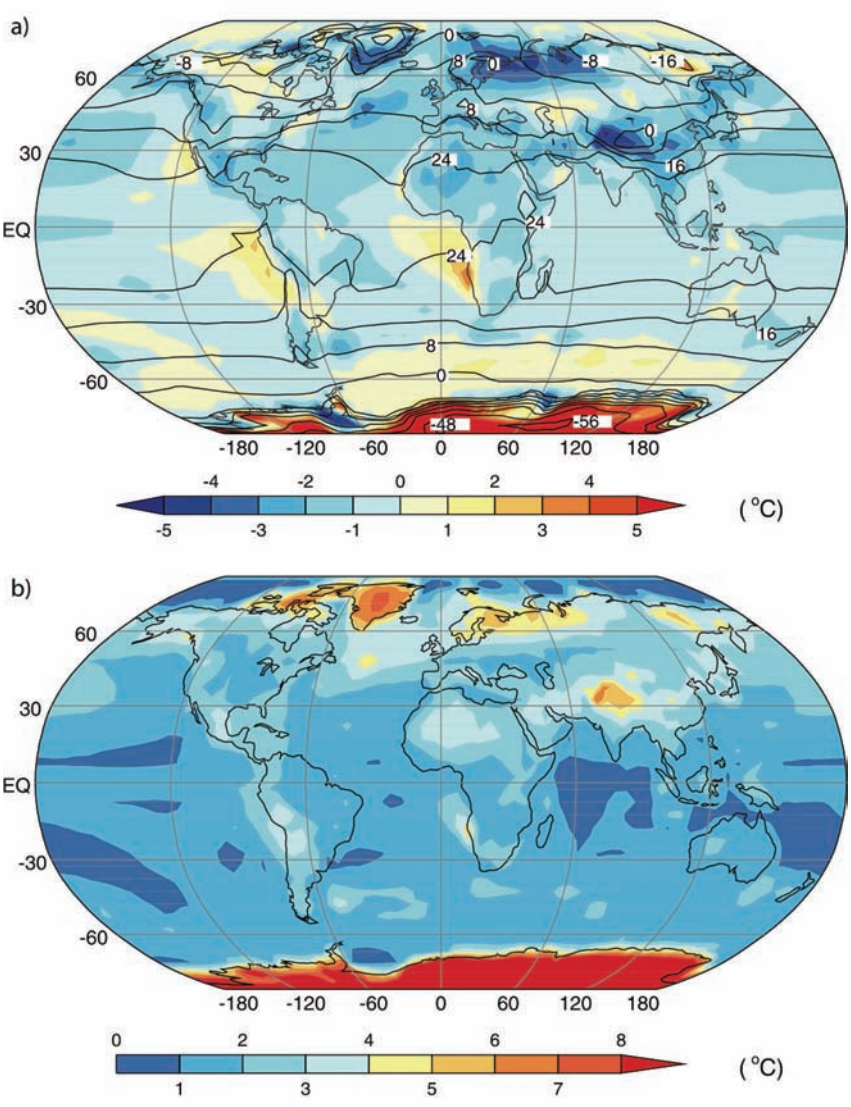

Figure 4.2: (a) Observed annual mean surface temperature (labelled contours) and the multi-model mean error for all 23 CMIP3 models, simulated minus observed (colour-shaded contours). Results are for 1960-1990 over land and 1980-1999 over the ocean. **(b)** Size of the typical model error, defined as the root-mean-square error computed over all simulations (from Figure 8.2 in Randall *et al*. 2007).

models were able to skillfully simulate many modes of climate variability, increasing confidence in their use for projecting climate change.

A simple measure of the ability of each model to simulate the Australian climate has been undertaken for the 23 models. This uses the non-dimensional measure of similarity 'M' (Watterson 1996) determined from the maps of simulated and observed seasonal-mean temperature, precipitation and sea level pressure. Observed temperature and precipitation data (on a 0.25 degree grid, approx. 25 km) come from the Australian Bureau of Meteorology, and observed pressure data (the 'ERA40' dataset) come from the European Centre for Medium Range Weather Forecasting. All data are interpolated to a common 0.25 degree Australian land grid. A single M value between 1 (perfect match) and 0 (no-skill) is obtained for each case, based on pattern correlations and root-mean-square errors. The average M skill scores for the three different variables across four seasons are given in Table 4.1. Fourteen models have skill scores between 0.6 and 0.7. Even the poorest performing model over Australia (GISS-EH) has some skill overall, with an average score of 0.3. These skill scores are used to weight climate projections from each model in Chapter 5. We assume that models with higher skill scores are likely to give more reliable projections of future climate.

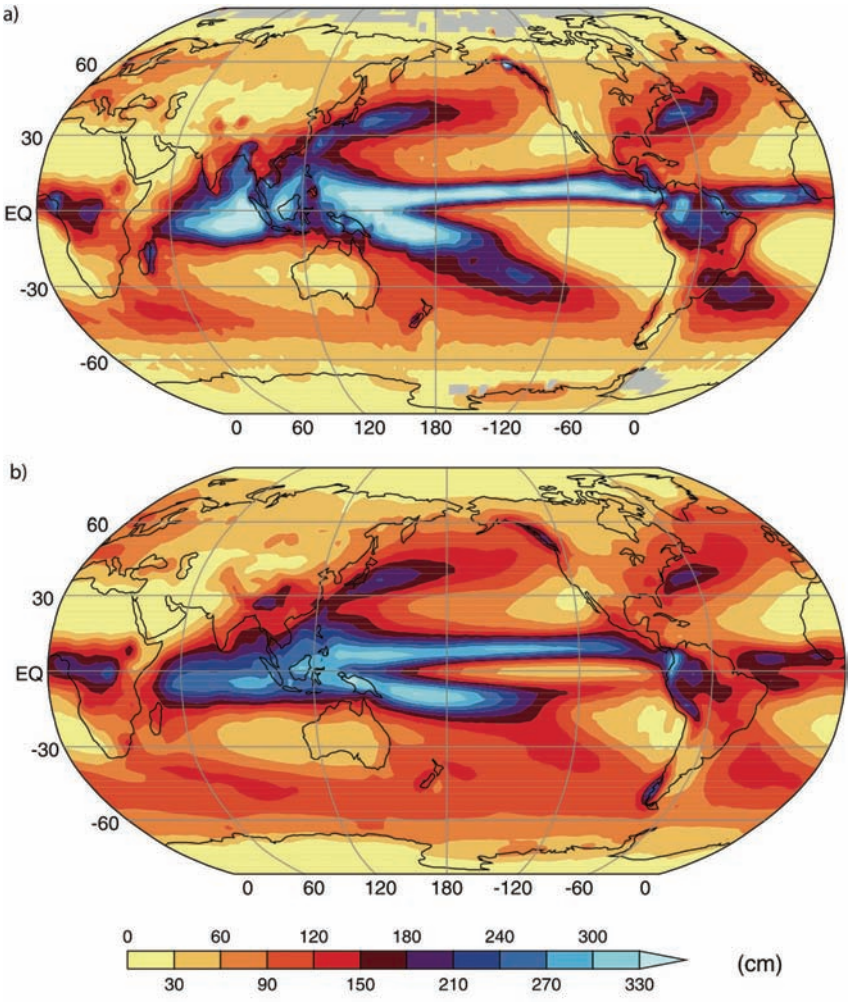

Figure 4.3: (a) Observed climatological annual mean precipitation and **(b)** multi-model mean precipitation from all 23 CMIP3 models. Observations are from Xie and Arkin (1997) updated for the period 1980-1999. Units are cm/year. (From Figure 8.5 in Randall *et al*. 2007)

4.2.4 Treatment of model uncertainties

Projections of global and regional climate change contain a large number of uncertainties. Predictability is limited by factors such as human behaviour and the uncertainties inherent in complex systems, such as chaotic behaviour and rapid changes in state. Uncertainty over future human behaviour affects emission scenarios, including future mitigation policies discussed in Section 4.1. Chaotic behaviour affects climate variability and change on a range of scales, from everyday variability (well understood) to long-term rapid shifts in climate (less common and not well understood but observable in palaeo-climate proxy records). Such behaviour is a long-term property of climate (and all complex systems) and may potentially increase under global warming (Schneider *et al*. 2007).

Structural uncertainty describes assumptions and system definitions, including how much of the actual system being simulated is included within a given modelling structure. Value uncertainty considers values, both as input and also how parameters and processes are represented within a model.

As mentioned in Chapter 1, techniques for combining model projections and producing conditional probabilities need to be very carefully managed. Over time, climate science has moved from producing single scenarios of some future state, often characterised as twice pre-industrial atmospheric CO_2, to large ensembles of transient climate change that can be portrayed as probability distributions.

The relationship between individual scenarios and ranges of change is shown in Figure 4.4 (Jones 2000; Ahmad *et al*. 2001). These show projected ranges with varying degrees of associated confidence. The well-calibrated range of uncertainty is typically quantified through a modelling exercise, whereas the judged range is more often constructed through expert judgement or other decision-analytic techniques (Ahmad *et al*. 2001). The total range of uncertainty acknowledges that uncertainties are often under-estimated by experts (Morgan and Henrion 1990).

The application of probabilities to the well-calibrated and even to the judged range of uncertainty can be justified if the above uncertainties are sufficiently well understood and managed, subject to the proviso that all such probabilities are understood to be conditional. The context, in this case, is that the IPCC has provided judged ranges of uncertainty each with attached likelihood representing their judgement that the 'true' answer is captured within that range (e.g. that climate projections correctly represent the response to specified forcing conditions) for variables such as global average warming and sea level rise. The derivation of estimates by the IPCC for global average warming is described in section 4.2.5 and conditional probability distributions are described in section 4.2.6. Chapter 5 describes the construction of regional projections of change for a range of variables, many of which include probability distributions.

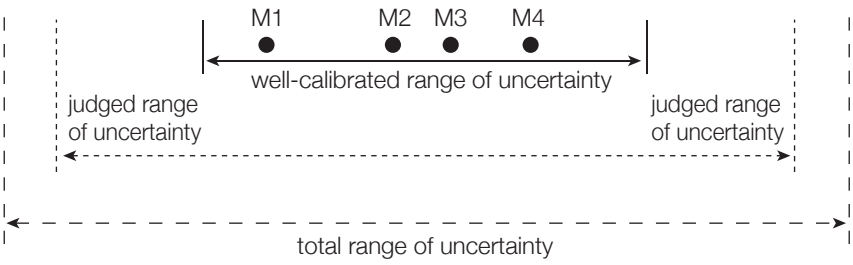

Figure 4.4: Schematic depiction of the relationship between well calibrated scenarios, the wider range of judged uncertainty that might be elicited through decision-analytic techniques and the full range of uncertainty, drawn wider to represent typical under-estimation in human judgements (Adapted from Jones 2000; Ahmad *et al*. 2001).

4.2.5 Global climate change projections for the 21st century

The 23 models in the CMIP3 dataset were driven by the B1, A1B and A2 emissions scenarios described in Box 4.1. This is a much larger set of simulations than was available for the IPCC Third Assessment Report in 2001, allowing better quantification of multi-model average changes, as well as uncertainty between models. Figure 4.5 shows the range of global warming for each of these scenarios, plus a hypothetical scenario applying constant year 2000 greenhouse gas concentrations. The IPCC (2007a) assessed the range of warming by the period 2090-2100, relative to 1980-1999, for the six SRES marker scenarios (B1, A1T, B2, A1B, A2 and A1FI) based on the 23 climate models, plus results from a hierarchy of independent models (complex, intermediate and simple) and observational constraints. Important uncertainties, including the possibility of significant further amplification of climate change due to carbon cycle feedbacks, are provided by the results of the Coupled Carbon Cycle Model Intercomparison Project (Friedlingstein *et al*. 2006). The lower end of the warming range (grey bars in Figure 4.5) corresponds to the mean warming minus 40%, while the upper end of the range is the mean warming plus 60%. The IPCC (2007a) global-average warming by 2090-2100 is 1.1-6.4ºC (Table 4.2).

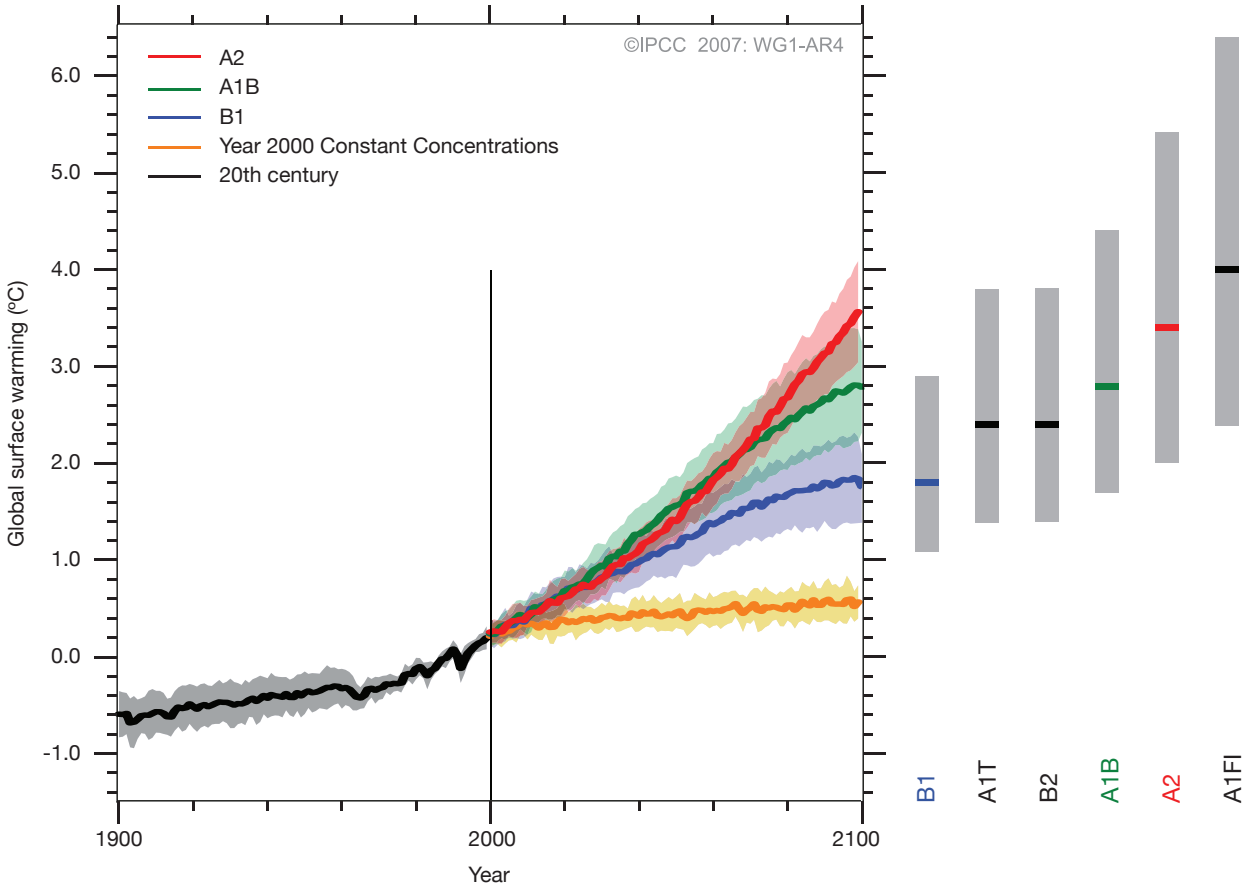

Figure 4.5: Global average warming (relative to 1980-99) for the scenarios A2, A1B and B1, shown as continuations of the 20th century simulations. Shading denotes the plus/minus one standard deviation range of individual model annual averages. The orange line is for the experiment where greenhouse gas concentrations were held constant at year 2000 values. The grey bars (right) indicate the multi-model mean warming (solid line within each bar) and the likely range of warming by the year 2100 for the six SRES marker scenarios, based on the A2, A1B and B1 simulations, plus results from independent models and observational constraints.(From IPCC (2007a) Fig SPM-5.)

Table 4.2: Best estimates and likely ranges of global warming for 2090-2099, relative to 1980-1999, for six SRES emission scenarios. (IPCC 2007a Table SPM-3).

Scenario	Best estimate	Likely range
B1	1.8°C	1.1-2.9°C
B2	2.4°C	1.4-3.8°C
A1T	2.4°C	1.4-3.8°C
A1B	2.8°C	1.7-4.4°C
A2	3.4°C	2.0-5.4°C
A1FI	4.0°C	2.4-6.4°C

Equivalent global warming estimates for 2030, 2050 and 2070 were not provided by the IPCC (2007a). Since these values are essential for the projections in Chapter 5, they have been derived in a manner consistent with the approach used by the IPCC for 2100 (Table 4.3). The multi-model mean global warmings for 2030, 2050 and 2070 were read from Figure 4.5 (or corresponding results from simple models). Note that these projections represent the anthropogenic change due to a specific change in radiative forcing for a period centred on a given year. Natural variability will influence actual values in any single year or decade.

The IPCC global warming ranges for 2100 (Meehl *et al*. 2007) are based on expert judgement in which multiple lines of evidence are taken into account. These include not only model results, but also estimates of climate sensitivity based on observed climate changes (coupled with estimates of radiative forcing) and palaeo-climate reconstructions. Warming outside these ranges cannot be excluded (Meehl *et al*. 2007, p 810). The range was described by the IPCC as 'likely'. From IPCC definitions, the likelihood of the true value being within the range is estimated to be at least 66% and less than 90%, but this percentage was not justified by the IPCC in this case. The IPCC concludes that the lower bound of the range is much better constrained than the upper bound. This is because the lower bound on climate sensitivity is better constrained and uncertainties in carbon cycle feedback are much less important for small temperature changes than for large ones (Meehl *et al*. 2007, p 810).

The ranges given in Table 4.3 were obtained simply by using -40% and +60% increments relative to the mean, as for 2100. This is supported by the statement of Meehl *et al*. (2007, p 809) that "projection uncertainties increase close to linearly with temperature in most studies", however the contribution of carbon cycle uncertainties may be smaller for the earlier times.

The IPCC also describes other 'Bayesian' approaches that estimate considerably smaller uncertainties of the 'real world' warming (Meehl *et al*. 2007). In particular, if one assumes that the model results are distributed about the 'true' value and improving in skill, then the uncertainty in the estimate of this value tends to decrease as the number of models considered increases, as is typical of statistical inference (Lopez *et al*. 2006). This issue will be also raised with respect to Australian regional changes in Chapter 5. In the results that follow, both the 'best estimates' and the likely ranges of uncertainty are derived directly from the global climate model ensemble, although the fitted range closely approximates the 'likely' range of global temperature change specified by the IPCC (Meehl *et al*. 2007). *Therefore, it must be borne in mind that, in particular, the upper limits of warming presented here and in Chapter 5 are conservative. There is a significant possibility that warming may occur in excess of these values, particularly later in the century, although the likelihood of this occurrence is impossible to estimate at this stage.*

It is worth noting that observed carbon dioxide concentrations, global mean temperatures and sea level rise have been tracking the upper end of the IPCC scenario range from 1990 to 2006 (Rahmstorf *et al*. 2007). Although this 17-year period is very short, it suggests that the mid and low projections may be less likely than the high projections, with significant implications for risk management.

Table 4.3: Global warming estimates [and representative ranges] relative to 1990 for selected years and emission scenarios. (Based on IPCC 2007a Figure SPM-3 and Meehl *et al*. 2007).

	2030	2050	2070
B1	0.75 [0.45-1.2]	1.1 [0.66-1.76]	1.5 [0.9-2.4]
B2	0.9 [0.54-1.44]	1.29 [0.77-2.06]	1.8 [1.08-2.88]
A2	0.8 [0.48-1.28]	1.4 [0.84-2.24]	2.25 [1.35-3.6]
A1B	0.9 [0.54-1.44]	1.53 [0.92-2.45]	2.13 [1.28-3.41]
A1T	1.0 [0.6-1.6]	1.7 [1.0-2.72]	2.2 [1.32-3.52]
A1F1	0.87 [0.52-1.39]	1.8 [1.08-2.88]	2.9 [1.74-4.64]

4.2.6 Deriving probability distributions for global warming

Varying global warming projections from climate models can be represented using probability distributions. These distributions are required for probabilistic regional climate change projections generated in Chapter 5.

Since probabilities were not provided by the IPCC (2007a), they have been derived using an approach that is similar to that used for local changes in Chapter 5. While this is based on an assessment of global climate model results for scenario A1B, described further by Watterson (2007), the results are quite consistent with the ranges of the previous section.

For the 22 individual models for which A1B simulations are available, the warming trend over the 21st century is evaluated by regression. The 100-year warming of each model from this analysis is given in Table 4.1. Further simulations of the same model would give somewhat different changes, and this will be particularly true of local results in Chapter 5. This uncertainty in the 'true' change of the model, as could be obtained by averaging over many simulations, can be estimated from the standard regression error. A probability density function (PDF) for the true individual model result is then a simple normal or Gaussian distribution, whose range is given by this error. Summing these individual normal distributions – one for each model (evenly weighted) – produces a combined probability density function, the 'Sum' curve plotted in Figure 4.6. The model with the largest warming stands out, here, but elsewhere there is some merging of the individual curves. The Sum PDF has the same mean as the warming in Table 4.2 (2.8ºC), and a similar range. If one randomly chose a new simulation from this set of models, this PDF would apply.

If we attempt to better represent the range of results from a typical model, or indeed the real world, it is reasonable to have a much smoother PDF. Figure 4.6 depicts the bell-shaped 'Normal' distribution, with the same mean and standard deviation as the Sum. The Normal 'fit' is however symmetric, even though the model results are somewhat 'skewed', with no small warmings. The IPCC ranges (Table 4.2) are also skewed. The 'Beta' distribution shown in Fig. 4.6 allows such skewness, but retaining the same mean and standard deviation. The tails of the Beta distribution in Figure 4.6 are constructed to extend slightly beyond the modelled range, and they also extend just beyond the range in Table 4.2 for this case (1.7-4.4ºC).

This Beta distribution gives a reasonable representation of simulated global warming for this emission scenario based on current climate models. Consistent with the ranges in Table 4.3, the same Beta distribution as in Figure 4.5 has been used to produce a PDF for the other years and scenarios, by scaling or stretching it by the ratio of the warming for the case and 2.8ºC.

For the purpose of providing probabilistic information in this report, we will assume that this set of PDFs also represents the uncertainty in real-world global warming for the various cases. As described in Chapter 5 and Watterson (2007), the projections for Australia will depend also on how the global warming PDFs are used, and the particular statistics presented. As noted at the end of section 4.2.5, *there is a significant possibility of future climate changes lying outside the projected ranges presented in this report, particularly so for changes associated with temperature increases at the upper end of the range, particularlly later in the century, although the likelihood of this occurrence is impossible to estimate at this stage.*

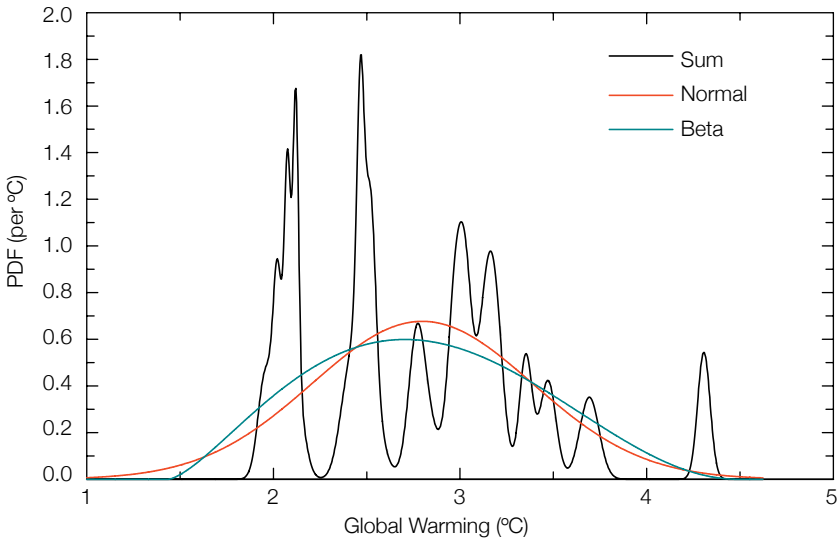

Figure 4.6: Probability distribution functions for the global mean warming for A1B over the 21st century, calculated from 22 models.

4.3 Global patterns of projected climate change of Australian relevance

It is important to place the Australian region projections contained in Chapter 5 in context of the large-scale patterns of change found in global models. Such patterns often display very large-scale coherence, and many of these large-scale changes can be understood from basic theoretical or physical constraints of the climate system, in particular related to increased ability of the atmosphere and increased moisture holding capacity (e.g. Held and Soden 2007). *Such constraints provide important extra confidence in projected regional changes, over and above that derived simply from the confidence placed in global climate models.*

The IPCC (2007a) report drew the following conclusions regarding regional patterns of climate change for the late 21st century:

- Greatest warming will occur over land and at high northern latitudes, and less warming will occur over the southern oceans and North Atlantic, consistent with observations during the latter part of the 20th century (Figure 4.7).
- Sea level pressure is projected to increase over the subtropics and mid-latitudes, and decrease over high latitudes due to a poleward expansion and weakening of the Hadley Circulation and a poleward shift of the storm tracks (Figure 4.7).
- Precipitation will generally increase in the wet tropics (such as the monsoon regimes) and over the tropical Pacific in particular, with general decreases expected in the subtropics, and increases at high latitudes due to the intensification of the hydrological cycle (Figure 4.7).
- Globally averaged mean water vapour, evaporation and precipitation are projected to increase.
- It is very likely that the duration, intensity and frequency of (i) heatwaves will increase, and (ii) cold periods and frosts will decline.
- Intensity of precipitation events is projected to increase, particularly in tropical and high latitude areas that experience increases in mean precipitation.
- Even in areas where mean precipitation decreases (most subtropical and mid-latitude regions), precipitation intensity is projected to increase but there would be longer periods between rainfall events.
- More frequent intense tropical cyclones, and associated extreme wind and rain are projected.
- A tendency for drying of the mid-continental areas during summer is expected to increase the risk of droughts in those regions.
- No consistent discernible change in ENSO frequency or intensity is evident in the projections.
- Snow cover and sea ice extent are expected to decrease, glaciers and ice caps are expected to lose mass, and this will contribute to further sea level rise.

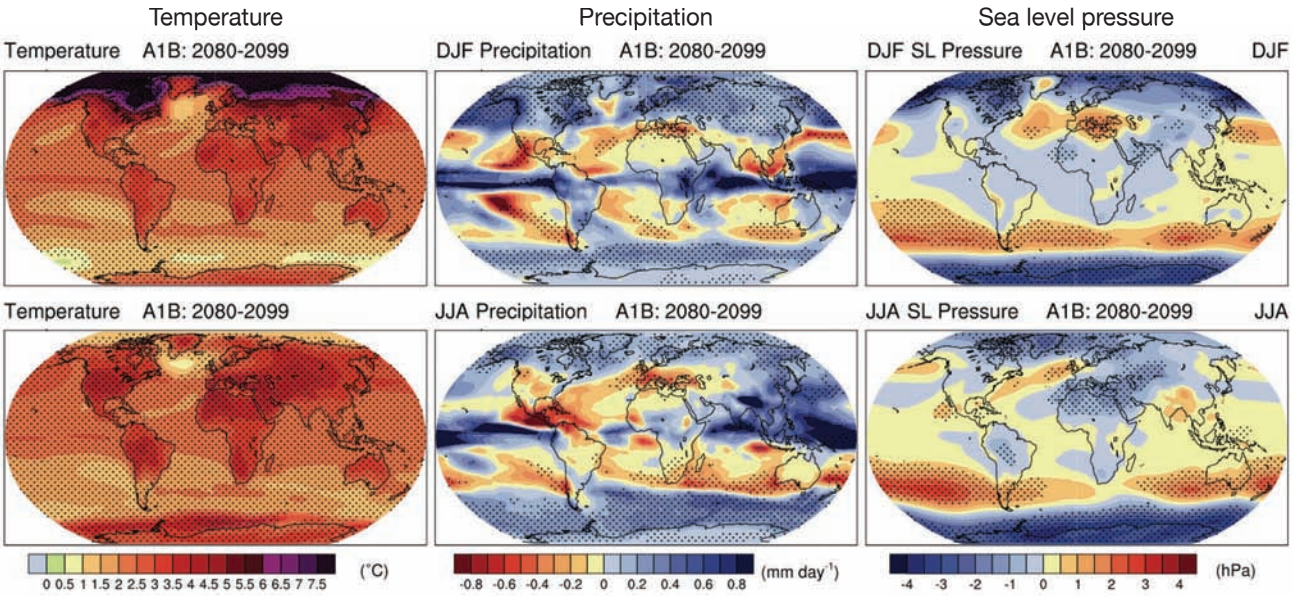

Figure 4.7: The global-average changes in surface temperature, precipitation and mean sea level pressure from 2080-2099, relative to 1980-1999. Based on the results of 20 climate models using the A1B scenario as an example, in December through February (DJF) and June through August (JJA), with shading indicating where the multi-models mean exceeds the inter-model standard deviation. (From Meehl *et al*. 2007 Figure 10.9.)